

RESEARCH ARTICLE

Open Access



Trace element partitioning between pyrochlore, microlite, fersmite and silicate melts

Stephan Klemme*  and Jasper Berndt

Abstract

We present experimentally determined trace element partition coefficients (D) between pyrochlore-group minerals ($\text{Ca}_2(\text{Nb,Ta})_2\text{O}_6(\text{O,F})$), Ca fersmite (CaNb_2O_6), and silicate melts. Our data indicate that pyrochlores and fersmite are able to strongly fractionate trace elements during the evolution of SiO_2 -undersaturated magmas. Pyrochlore efficiently fractionates Zr and Hf from Nb and Ta, with D_{Zr} and D_{Hf} below or equal to unity, and D_{Nb} and D_{Ta} significantly above unity. We find that D_{Ta} pyrochlore-group mineral/silicate melt is always higher than D_{Nb} , which agrees with the HFSE partitioning of all other Ti-rich minerals such as perovskite, rutile, ilmenite or Fe-Ti spinel. Our experimental partition coefficients also show that, under oxidizing conditions, D_{Th} is higher than corresponding D_{U} and this implies that pyrochlore-group minerals may fractionate U and Th in silicate magmas. The rare earth element (REE) partition coefficients are around unity, only the light REE are compatible in pyrochlore-group minerals, which explains the high rare earth element concentrations in naturally occurring magmatic pyrochlores.

Keywords: Pyrochlore, Microlite, Nb, Ta, Ore deposit, Fersmite, Trace element, Partition coefficients, Alkaline rocks, Experimental petrology, LA-ICP-MS, Electron microprobe

Introduction

To understand the behavior of trace elements in igneous rocks, trace element partition coefficients between minerals and melts are needed. Over the last decades, numerous experimental studies focused on the trace element partitioning between major rock forming minerals and melts [1], but few experimental partition coefficients are available for accessory phases such as rutile, ilmenite, spinel or apatite in basaltic compositions [2–12] and even less data are available for accessory mineral phases such as perovskite or pyrochlore in alkaline rock compositions [13]. As the aforementioned accessory mineral phases commonly occur in alkaline igneous rocks, they may exert a strong control on the trace element evolution of alkaline magmas.

In this study we focus on the Nb- and Ta-rich accessory phases pyrochlore, microlite, and fersmite, which are accessory phases in alkaline silicate rocks [14–20] and, perhaps more commonly, carbonatites [18, 21–23]. Note that these mineral phases are the most important hosts for Nb and Ta in ore deposits (e.g., [18, 24–27]).

The pyrochlore-group of minerals in silicate rocks and carbonatites encompasses a very large and very complex group of minerals [28]. The general formula of minerals of the pyrochlore supergroup is $\text{A}_2\text{B}_2\text{O}_7$, where the A-site is often occupied by monovalent or divalent cations, and the B-site is mainly occupied by pentavalent cations such as Nb or Ta. Pyrochlore *sensu stricto* is a mineral in which the B-site is occupied by Nb, and microlites are minerals in which the B-site is occupied by Ta [28]. We do not aim to describe the entire compositional variability of pyrochlores and related minerals in alkaline rocks, and we would like to refer the interested reader to excellent papers by Mitchell, Chakhmouradian, and others [18,

*Correspondence: stephan.klemme@uni-muenster.de
Institut für Mineralogie, Universität Münster, Corrensstraße 24,
48149 Münster, Germany



21, 22, 26, 29–33]. However, common accessory mineral phases in carbonatites and alkaline silicate rocks are Ca-Na pyrochlores that can (and often do) incorporate almost all geochemical indicator elements, including the rare earth elements (REE), the large ion lithophile elements (e.g., K and Ba), and, as they are Nb- and Ta-rich minerals, also the high field strength elements Nb, Ta, Zr, and Hf (e.g., [21, 22, 26, 30, 31, 33, 34]).

As there are, to our knowledge, no previous experimental studies on the partitioning of trace elements between pyrochlore-group minerals and melts, we set out to determine trace element partition coefficients between pyrochlore ($\text{Ca}_2\text{Nb}_2\text{O}_7$), microlite ($\text{Ca}_2\text{Ta}_2\text{O}_7$), fersmite (CaNb_2O_6), and silicate melts. The long-term objective of this work is to determine the effects of temperature, pressure, and perhaps most importantly, chemical composition of minerals on trace element partition coefficients. Hence future experiments will be extended towards systems with carbonate melts. Our experiments presented here were done in simplified chemical compositions, and must hence be considered as a first step towards a better understanding of trace element partitioning in complex natural systems where pyrochlore-group minerals occur.

Experimental and analytical methods

Starting materials

To ensure the nucleation and growth of pyrochlore-group minerals and fersmite to a reasonable size and, thus, enabling in-situ analysis by laser ablation inductively-coupled plasma mass spectrometry (LA-ICP-MS), we conducted a few exploratory experiments to establish chemical compositions which precipitated pyrochlore-group minerals and fersmite. In order to avoid possible experimental problems related to Fe-loss, all starting materials did not contain Fe. Starting material SM_Pyro1 is a composition in the system $\text{CaO-Na}_2\text{O-Al}_2\text{O}_3\text{-SiO}_2\text{-Nb}_2\text{O}_5\text{-F}$, and HWM in the system

$\text{CaO-Na}_2\text{O-Al}_2\text{O}_3\text{-SiO}_2\text{-Ta}_2\text{O}_5$. The choice of this rather simple chemical composition was made after our reconnaissance experiments in more complex systems yielded only small Nb-mineral crystals (<15 μm), which were impossible to analyze with our LA-ICP-MS set-up. Both starting materials were prepared from analytical grade oxides, hydroxides, and carbonates (Table 1), which were ground in an agate mortar under ethanol. The starting material mixtures were heated in air at 1000 °C for 3 h in order to ensure complete decarbonation. Subsequently, the mixtures were heated to temperatures well above 1600 °C (10 min), i.e. above the liquidus in these systems, quenched, and the resulting glasses were re-ground to fine powders. All starting materials (except in run SE_Pyro2, see below) were doped with a trace element mixture (SKM-TE1) containing the following elements: La, Ce, Nd, Sm, Gd, Dy, Yb, Lu, Y, Li, Sr, Ba, Rb, Sc, Mn, Ni, Co, Mo, Te, Ga, Ge, In, Cr, Zr, Nb, Hf, Ta, Pb. U and Th were added separately using 1000 $\mu\text{g/g}$ ICP-AES standard (Alfa Aesar, in diluted nitric acid) solutions. The starting material compositions are given in Table 1. Note that run SE_Pyro2 was an exploratory run to which no trace elements were added. The doped starting materials were subsequently dried and denitrified in a laboratory-type drying cabinet at 110 °C (12 h).

Experimental techniques

All experiments were run in conventional 1-atmosphere vertical furnaces in air [11], using the Pt-wire loop technique (e.g., [11, 13, 35–37]). To prepare the loops, we mixed about 20 mg of starting material powder into a viscous slurry with a synthetic glue, and we loaded this mixture onto a 0.1 mm diameter Pt-wire loop. The samples were then introduced into the hotspot of a vertical alumina tube furnace (Gero GmbH, Germany). Temperature was controlled with a thermocouple external to the alumina tube by a Eurotherm controller,

Table 1 Starting materials

| | SM_Pyro1 | HWM | SKM-TE1 | | | | | | | |
|-------------------------|----------|------|---------|-----|------|-----|------|-----|------|-----|
| | wt.% | wt.% | wt.% | | wt.% | | wt.% | | wt.% | |
| Na_2O | 1.1 | 0.9 | La | 2.8 | Lu | 3.0 | Sr | 2.2 | Ga | 1.6 |
| CaO | 24.8 | 28.9 | Ce | 2.6 | Y | 2.3 | Pb | 6.8 | Ge | 7.6 |
| Al_2O_3 | 6.7 | 3.8 | Nd | 3.6 | Zr | 6.0 | Mn | 2.3 | In | 2.6 |
| SiO_2 | 19.7 | 21.6 | Sm | 7.0 | Hf | 6.6 | Ni | 3.0 | Cr | 1.6 |
| Nb_2O_5 | 44.7 | – | Gd | 2.8 | Nb | 3.0 | Co | 5.7 | Li | 0.4 |
| Ta_2O_5 | – | 44.8 | Dy | 2.7 | Ta | 4.6 | Mo | 5.7 | Ba | 2.9 |
| F | 3.0 | – | Yb | 2.3 | Rb | 4.2 | Te | 1.5 | Sc | 2.4 |
| total | 100 | 100 | | | | | | | | |

Note that the trace element mixture SKM-TE1 was added to both starting materials SM_Pyro1 and HWM, only run SE_Pyro2 was run without trace elements. See text for details

limiting fluctuations to within 1 °C. The temperature was additionally monitored with a Type B thermocouple (Pt₇₀Rh₃₀-Pt₉₄Rh₆) close to the sample. The runtime (at final run temperature) varied between 20 and 120 h (see Table 2 for details). After quenching of the experimental charges, the samples were embedded in epoxy resin and polished using several different diamond pastes, and carbon coated for qualitative and quantitative analysis.

Analytical techniques

The experimental run products were examined with a JEOL6610LV scanning electron microscope with an EDX system and the major element concentrations of all phases were determined with a 5-spectrometer JEOL JXA 8530F electron microprobe analyzer (EMPA) at the Institut für Mineralogie at the University of Münster. Mineral phases were analyzed using beam spot sizes between 2–5 µm at a current of 15 nA. Counting times were 20 s on the peak and 10 s on the background. Glasses and quenched melts were analyzed with a 10 µm defocused beam and counting times were 5 s on the peak and 3 s on the background to minimize loss of volatile elements. Matrix-matched minerals were used as reference materials. Additionally, a set of secondary standards was measured together with the unknowns to monitor external precision and accuracy [38]. Trace elements were analyzed using a LA-ICP-MS system at the University of Münster that consisted of an Element 2 (ThermoFisher Scientific) SF-ICP-MS connected to a 193 nm ArF excimer laser ablation system (Teledyne Photon Machines Analyte G2). Laser repetition rate was 5 Hz using an energy density of about 4 J/cm². Prior to sample analyses, the system was tuned with the NIST SRM 612 standard for high sensitivity, stability, and low oxide rates (²³²Th/¹⁶O/²³²Th < 0.1%). Ablation time was 40 s and the background was measured for 20 s prior to sample ablation. Spot size was 12–25 µm for pyrochlores

and fersmite crystals and melts, and 35 µm for the reference materials. ⁴³Ca was used for internal calibration and NIST SRM 612 was chosen as the external standard using concentration values given in the GeoRem database, version 26/2019 [39]. Groups of 8–17 spot analyses were bracketed by three standard analyses to monitor instrumental drift. All concentrations were calculated using the Glitter software (version 4.4.4 [40]). Standard reference glasses BCR2-G, BIR1-G, and BHVO2-G were analyzed as monitor for precision and accuracy for silicate phases during the course of this study. Obtained results match the published range of concentrations given in the GeoRem database [39].

Results and discussion

Experimental results

The experiments (Table 2) yielded euhedral-to-subhedral pyrochlore and fersmite crystals from < 15 µm up to about 150 µm across. In some runs, pyrochlore or fersmite crystal were thin and acicular so that they could not be analyzed with LA-ICPMS (c.f., Table 2). No other crystals were observed. The melt quenched to a dark and inclusion-free homogeneous glass. Electron microprobe and LA-ICP-MS analyses of pyrochlore and fersmite crystals and quenched melts indicate major- and trace element homogeneity, which is taken as evidence for the attainment of equilibrium between crystals and melts in our runs. Representative run products are shown in Fig. 1.

We would like to note that the exploratory experiment SE_Pyro2 was run with a starting material that did not contain added trace elements. Consequently, the trace element concentrations in both minerals and quenched melts in this run are substantially lower than in all other experiments (Table 2). However, the partition coefficients of this run are in excellent agreement with D's from the other runs (see discussion below, Table 4), which

Table 2 Experimental conditions and run products

| Run no | T/°C start | Cooling rate °/min | T/°C end | Duration (h) at T end | Starting material | Phases present |
|----------|------------|--------------------|----------|-----------------------|-------------------|-------------------|
| SE_Pyro2 | 1400 | 100 | 1300 | 24 | SM_Pyro1 | Fer, Nb-pyr, melt |
| SE_Pyro3 | 1400 | 20 | 1300 | 24 | SM_Pyro1 | Fer, Nb-pyr, melt |
| SE_Pyro5 | 1400 | 10 | 1260 | 24 | SM_Pyro1 | Fer, Nb-pyr, melt |
| SE_Pyro6 | 1400 | 5 | 1240 | 120 | SM_Pyro1 | Fer, Nb-pyr, melt |
| HW1 | 1400 | 0.1 | 1300 | 28 | HWM | Ta-pyr, melt |
| HW2 | 1350 | 0.2 | 1200 | 20 | HWM | Ta-pyr, melt |
| HW3 | 1400 | – | 1400 | 46 | HWM | Ta-pyr, melt |

Fer=Ca-Nb-fersmite; Nb-pyr=Ca-Nb-pyrochlore; melt=quenched melt; Ta-pyr=Ca-Ta-microlite

Note that in run HW3 no cooling rate was used. Note also that fersmite in runs SE_Pyro3, and pyrochlores in SE_Pyro2 were acicular and too small for EMPA analysis. All experiments were run in air and at atmospheric pressure. T/°C start: T at which the samples were inserted into the furnace, T/°C end: The temperature of the run after the cooling rate; cooling rate: The samples were cooled from T_{start} to T_{end}, and the runs were held at T_{end} for at least 20 h (duration (h) at T_{end})

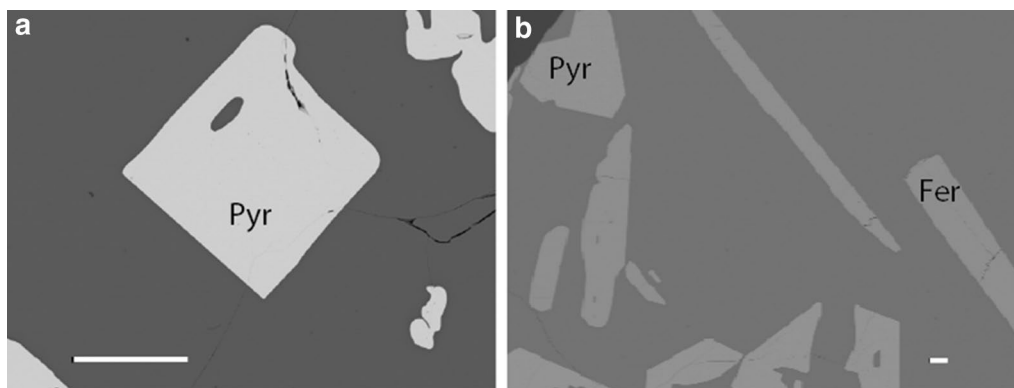


Fig. 1 Back-scattered electron images taken with the SEM. The white horizontal scale bar is 100 μm in both images. A: run product HW2 contains pyrochlore surrounded by quenched melt. B: run SE_Pyro_6 contains both fersmite (fer), pyrochlore (pyr), and quenched melt

confirms the quality of our trace element analyses at very low concentrations, and also that Henry's law has been attained [41].

Analytical results

Major, minor and trace elements of all phases were analyzed using EPMA and LA-ICPMS techniques, and the analytical results are given in Tables 3 and 4. Note that some of the crystals (Table 2) were too small to be analyzed.

Partition coefficients

The trace element concentrations of pyrochlore, microlite, and fersmite crystals and quenched melts were used to calculate trace element partition coefficients (D_i) using the following expression:

$$D_i = c_{i,\text{min}} / c_{i,\text{melt}}$$

where D_i is the partition coefficient for a trace element i , $c_{i,\text{min}}$ is the measured concentration of the trace element i in the crystal, and $c_{i,\text{melt}}$ is the concentration of the trace element i in the melt. The calculated trace element partition coefficients together with the propagated uncertainties, are given in Table 4, and are depicted in Fig. 2.

The light element Li is incompatible, with partition coefficients slightly less than unity. The divalent elements Sr and Mn partition evenly between pyrochlore, fersmite and silicate melt, with partition coefficients slightly less than unity, the D 's for Ni and Co are slightly lower (Fig. 2, Table 4). The Ge partition coefficients are all slightly below or close to unity (Fig. 2, Table 4), indicating that Ge follows the geochemical behavior of Si. Sc and Ba partition coefficients cluster around 0.1, with no apparent systematics (Fig. 2).

The partition coefficients of the rare earth elements (REE and Y) are depicted in Fig. 3. Our results show that D_{REE} pyrochlore/melt increases with decreasing ionic radius of the REE. The light REE (LREE) La, Ce, Pr, Sm and Gd are compatible in pyrochlore in all runs, regardless of temperature or bulk composition. The D_{REE} pyrochlore/melt of the heavier REE (Yb, Lu, and also Y) are slightly below 1, in run HW3 all D_{REE} are above 1. Our data shows that the D_{REE} of Ta-rich pyrochlores (i.e. the HW1-HW3 runs, black filled symbols in Fig. 3) are systematically higher than the D_{REE} from experiments with Nb-rich pyrochlores (runs SE3 and SE6, open triangles in Fig. 3). As the REE are incorporated on the Ca-site in pyrochlores, the different partitioning may be explained by the different nature of the Ca-site in Ta-rich (i.e. microlite) and Nb-rich pyrochlores, respectively. Crystallographic data show that the size of the Ca-site in Nb-rich pyrochlore is slightly smaller (average Ca-O bond length in pyrochlore of 2.58 Å [42]) than the Ca-site in Ta-pyrochlore (microlite), with an average Ca-O bond length of 2.73 Å [43].

If we only consider the D_{REE} of the Ta-rich microlites (i.e. the HW runs), we find that D_{REE} of HW3, which was run at 1400 °C, is substantially higher than D 's of runs HW2 and HW1 which were run at a final run temperature of 1300° and 1200 °C. However, the D 's of HW1 and HW2 are undistinguishable within the errors and hence the temperature effect on D 's cannot be fully confirmed.

The D_{REE} fersmite/melt show a much flatter and only slightly downwards concave pattern, with $D_{\text{La}}/D_{\text{Lu}}$ very close to unity, and D_{REE} of the middle REE (Nd, Sm, Gd, Dy) slightly higher than the D_{LREE} or D_{HREE} , similar to D_{REE} between apatite and melt (e.g., [44]). This clearly indicates that the nature of the Ca-site in fersmite is quite different to that of microlite or pyrochlore, and crystallographic data confirm that the

Table 3 Major element compositions of minerals and melts

| n | 5 | | 8 | | 10 | | 10 | | | | | |
|--------------------------------|----------|-------|----------|-------|----------|-------|----------|-------|----------|-------|------|-------|
| | SE_Pyro2 | | SE_Pyro2 | | SE_Pyro3 | | SE_Pyro3 | | | | | |
| | Fer | | Melt | | Nb-Pyr | | Melt | | | | | |
| | av | Stdev | av | Stdev | av | Stdev | av | Stdev | av | Stdev | av | Stdev |
| Na ₂ O | n.d | | 0.4 | 0.04 | | | 0.24 | 0.08 | | | | |
| Al ₂ O ₃ | n.d | | 5.4 | 0.5 | | | 5.2 | 0.1 | | | | |
| CaO | 17.4 | 0.5 | 31.3 | 0.8 | 28.6 | 0.4 | 31.3 | 0.8 | | | | |
| SiO ₂ | n.d | | 28.2 | 0.2 | | | 28.2 | 0.2 | | | | |
| Ta ₂ O ₅ | n.a | | n.a | | n.a | | n.a | | | | | |
| Nb ₂ O ₅ | 80.8 | 0.03 | 30.7 | 0.1 | 68.4 | 0.2 | 30.7 | 0.1 | | | | |
| F | 0.9 | 0.2 | 3.5 | 0.5 | 2.6 | 0.4 | 2.6 | 0.2 | | | | |
| Total | 99.1 | | 99.50 | | 99.60 | | 98.2 | | | | | |
| n | 3 | | 10 | | 2 | | 8 | | 10 | | | |
| | SE_Pyro5 | | SE_Pyro5 | | SE_Pyro6 | | SE_Pyro6 | | SE_Pyro6 | | | |
| | Fer | | Melt | | Fer | | Nb-Pyr | | Melt | | | |
| | av | Stdev | av | Stdev | av | Stdev | av | Stdev | av | Stdev | av | Stdev |
| Na ₂ O | n.d | | n.d | | n.d | | n.d | | n.d | | | |
| Al ₂ O ₃ | n.d | | 6.1 | 0.9 | n.d | | n.d | | 6.3 | 0.1 | | |
| CaO | 17.1 | 0.3 | 32.5 | 0.5 | 17.3 | 0.5 | 29.0 | | 32.7 | 0.2 | | |
| SiO ₂ | n.d | | 32.3 | 0.4 | n.d | | n.d | | 33.7 | 0.3 | | |
| Ta ₂ O ₅ | n.a | | n.a | | n.a | | n.a | | n.a | | | |
| Nb ₂ O ₅ | 82.8 | 0.4 | 23.1 | 0.7 | 80.8 | 0.5 | 67.7 | | 21.8 | 0.4 | | |
| F | 0.5 | 0.2 | 4.2 | 0.6 | 0.8 | 0.3 | 2.4 | | 3.1 | 0.3 | | |
| Total | 100.4 | | 98.2 | | 98.9 | | 99.2 | | 97.6 | | | |
| n | 10 | | 10 | | 10 | | 10 | | 10 | | 10 | |
| | HW1 | | Melt | | HW2 | | Melt | | HW3 | | Melt | |
| | Ta-pyr | | Melt | | Ta-pyr | | Melt | | Ta-pyr | | Melt | |
| | av | Stdev | av | Stdev | av | Stdev | av | Stdev | av | Stdev | av | Stdev |
| Na ₂ O | 0.06 | 0.03 | 0.4 | 0.1 | 0.05 | 0.03 | 0.52 | 0.03 | 0.12 | 0.03 | 4.2 | 0.1 |
| Al ₂ O ₃ | 0.04 | 0.01 | 6.5 | 0.1 | 0.04 | 0.02 | 5.78 | 0.11 | 0.03 | 0.02 | 14.7 | 0.1 |
| CaO | 20.1 | 0.2 | 37.2 | 0.5 | 20.1 | 0.1 | 35.2 | 0.3 | 19.9 | 0.2 | 25.0 | 0.4 |
| SiO ₂ | 0.04 | 0.03 | 41.1 | 0.7 | 0.05 | 0.04 | 37.2 | 0.2 | 0.04 | 0.03 | 45.0 | 0.4 |
| Ta ₂ O ₅ | 79.3 | 0.5 | 15.5 | 1.0 | 79.2 | 0.6 | 21.7 | 0.2 | 79.9 | 0.8 | 10.1 | 0.8 |
| Nb ₂ O ₅ | 0.13 | 0.05 | 0.09 | 0.04 | 0.13 | 0.04 | 0.1 | 0.1 | 0.10 | 0.05 | 0.02 | 0.01 |
| Total | 99.6 | 0.5 | 100.7 | 2.4 | 99.6 | 0.9 | 100.4 | 0.9 | 100.0 | 1.1 | 99.0 | 1.8 |

Major element composition of minerals and quenched melts (Fer = Ca-Nb-fernsmite, Nb-pyr = Ca-Nb-pyrochlore, melt = quenched melt, Ta-pyr = Ca-Ta-microlite) analyzed with EMPA. *n* number of analyses, *n.d.* not detected, *n.a.* not analyzed. Note that fersmite occurred in all runs with the SE_Pyro1 starting materials (Table 1) but in most runs these crystals were too small to be analyzed, and we only present data from runs SE_Pyro5 and SE_Pyro6.

size of the Ca-site is much smaller in fersmite (average Ca-O bond lengths 2.4 Å [45]) than in pyrochlore (average Ca-O bond lengths 2.58 Å [42]). Furthermore, the Ca-site in pyrochlore is eightfold coordinated [42], but the Ca-site in fersmite is smaller and sixfold coordinated [45]. We find that D_{REE} fersmite/melt are highest in run SE_Pyro2, which was run at the highest final run

temperature of 1300 °C, whereas run SE_Pyro6, which was run at 1240 °C, resulted in the lowest D_{REE} .

Our data clearly shows that Ce is much more compatible than neighboring REE in runs with the HW starting material, which does not contain F. We can explain the deviant behavior of Ce in these runs, as Ce is a multi-valent trace element and under oxidizing conditions Ce

Table 4 Trace element compositions of minerals and melts, and calculated partition coefficients

| n | HW1 | | | | | |
|----|---------|--------|---------|-------|--------------|-------|
| | 7 | | 6 | | D Ta-pyr HW1 | Stdev |
| | Ta-Pyr | Stdev | Melt | Stdev | | |
| Li | 1.0 | 0.1 | 12.7 | 0.3 | 0.08 | 0.01 |
| Sc | 205 | 22 | 1100 | 14 | 0.19 | 0.02 |
| Mn | 101 | 11 | 290 | 1 | 0.35 | 0.04 |
| Co | 205 | 37 | 1290 | 10 | 0.16 | 0.03 |
| Ni | 76 | 16 | 641 | 4 | 0.12 | 0.03 |
| Ga | 21 | 11 | 791 | 13 | 0.03 | 0.01 |
| Ge | 77 | 10 | 250 | 4 | 0.31 | 0.04 |
| Sr | 187 | 3 | 477 | 3 | 0.39 | 0.01 |
| Y | 708 | 105 | 707 | 4 | 1.0 | 0.1 |
| Zr | 896 | 130 | 906 | 8 | 1.0 | 0.1 |
| Nb | 999 | 92 | 777 | 12 | 1.3 | 0.1 |
| Mo | 0.20 | 0.18 | 12.8 | 0.2 | 0.02 | 0.01 |
| Ba | 33 | 9 | 736 | 7 | 0.04 | 0.01 |
| La | 1111 | 173 | 448 | 6 | 2.5 | 0.4 |
| Ce | 1070 | 361 | 191 | 3 | 5.6 | 1.9 |
| Nd | 1695 | 389 | 490 | 8 | 3.5 | 0.8 |
| Sm | 1408 | 323 | 466 | 4 | 3.0 | 0.7 |
| Gd | 675 | 127 | 317 | 3 | 2.1 | 0.4 |
| Dy | 565 | 91 | 372 | 2 | 1.5 | 0.2 |
| Yb | 324 | 37 | 487 | 3 | 0.7 | 0.1 |
| Lu | 558 | 64 | 1048 | 11 | 0.5 | 0.1 |
| Hf | 1390 | 299 | 782 | 14 | 1.8 | 0.4 |
| Ta | 590,712 | 27,309 | 121,645 | 5874 | 4.9 | 0.3 |
| Th | 0.5 | 0.2 | 0.06 | 0.01 | 7.8 | 3.1 |
| U | 1.6 | 0.3 | 4.0 | 0.1 | 0.4 | 0.1 |

| n | HW2 | | | | | |
|----|--------|-------|------|-------|--------------|-------|
| | 8 | | 6 | | D Ta-pyr HW2 | Stdev |
| | Ta-Pyr | Stdev | Melt | Stdev | | |
| Li | 1.4 | 0.2 | 14.3 | 0.4 | 0.10 | 0.02 |
| Sc | 187 | 25 | 985 | 10 | 0.19 | 0.03 |
| Mn | 105 | 4 | 282 | 7 | 0.37 | 0.02 |
| Co | 208 | 18 | 1197 | 12 | 0.17 | 0.01 |
| Ni | 77 | 11 | 581 | 6 | 0.13 | 0.02 |
| Ga | 18 | 5 | 705 | 9 | 0.03 | 0.01 |
| Ge | 70 | 8 | 60 | 2 | 1.18 | 0.13 |
| Sr | 180 | 3 | 448 | 5 | 0.40 | 0.01 |
| Y | 678 | 73 | 674 | 16 | 1.01 | 0.11 |
| Zr | 834 | 116 | 933 | 16 | 0.89 | 0.13 |
| Nb | 899 | 45 | 882 | 10 | 1.02 | 0.05 |
| Mo | 0.09 | 0.04 | 6.2 | 0.2 | 0.015 | 0.007 |
| Ba | 30 | 4 | 660 | 7 | 0.05 | 0.01 |
| La | 1067 | 74 | 481 | 5 | 2.2 | 0.2 |
| Ce | 1053 | 203 | 240 | 4 | 4.4 | 0.9 |
| Nd | 1693 | 212 | 543 | 7 | 3.1 | 0.4 |
| Sm | 1388 | 178 | 503 | 8 | 2.8 | 0.4 |
| Gd | 662 | 74 | 329 | 5 | 2.0 | 0.2 |

Table 4 (continued)

| HW2 | | | | | | |
|-----------------|---------------|--------------|-------------|--------------|--------------------------|--------------|
| n | 8 | | 6 | | | |
| | Ta-Pyr | Stdev | Melt | Stdev | D Ta-pyr HW2 | Stdev |
| Dy | 550 | 57 | 371 | 6 | 1.5 | 0.2 |
| Yb | 318 | 30 | 450 | 7 | 0.7 | 0.1 |
| Lu | 545 | 45 | 964 | 15 | 0.57 | 0.05 |
| Hf | 1326 | 202 | 848 | 18 | 1.6 | 0.2 |
| Ta | 603,553 | 6796 | 167,305 | 2991 | 3.6 | 0.1 |
| Th | 0.5 | 0.1 | 0.080 | 0.004 | 5.9 | 1.5 |
| U | 0.9 | 0.1 | 3.56 | 0.03 | 0.26 | 0.02 |
| HW3 | | | | | | |
| n | 6 | | 5 | | | |
| | Ta-Pyr | Stdev | Melt | Stdev | D Ta-pyr HW3 | Stdev |
| Li | 3.2 | 0.6 | 68 | 21 | 0.05 | 0.02 |
| Sc | 112.8 | 48.9 | 1053 | 333 | 0.11 | 0.06 |
| Mn | 66.5 | 19.5 | 517 | 152 | 0.13 | 0.05 |
| Co | 109.5 | 43.9 | 3013 | 988 | 0.04 | 0.02 |
| Ni | 33.4 | 18.1 | 1409 | 456 | 0.024 | 0.015 |
| Ga | 10.5 | 1.2 | 1915 | 608 | 0.005 | 0.002 |
| Ge | 85.3 | 8.3 | 1340 | 419 | 0.06 | 0.02 |
| Sr | 196.5 | 6.5 | 904 | 291 | 0.22 | 0.07 |
| Y | 717.7 | 41.7 | 235 | 69 | 3.1 | 0.9 |
| Zr | 665.9 | 127.1 | 208 | 59 | 3.2 | 1.1 |
| Nb | 831.0 | 13.7 | 487 | 148 | 1.7 | 0.5 |
| Mo | 1.2 | 0.1 | 70 | 23 | 0.017 | 0.006 |
| Ba | 34.1 | 2.2 | 1843 | 570 | 0.018 | 0.006 |
| La | 1417 | 231 | 509 | 154 | 2.8 | 1.0 |
| Ce | 1527 | 269 | 87 | 24 | 17.6 | 5.8 |
| Nd | 2235 | 305 | 332 | 93 | 6.7 | 2.1 |
| Sm | 1770 | 171 | 251 | 71 | 7.1 | 2.1 |
| Gd | 778 | 35 | 138 | 39 | 5.6 | 1.6 |
| Dy | 608 | 18 | 138 | 40 | 4.4 | 1.3 |
| Yb | 304 | 31 | 148 | 43 | 2.0 | 0.6 |
| Lu | 493 | 66 | 319 | 94 | 1.5 | 0.5 |
| Hf | 1054 | 300 | 367 | 104 | 2.9 | 1.2 |
| Ta | 589,199 | 9317 | 87,900 | 24,870 | 6.7 | 1.9 |
| Th | 0.8 | 0.2 | 0.10 | 0.03 | 7.8 | 3.0 |
| U | 1.5 | 0.3 | 12 | 4 | 0.12 | 0.04 |
| SE_Pyro3 | | | | | | |
| n | 5 | | 5 | | | |
| | Nb-pyr | Stdev | Melt | stdev | D Nb-pyr/melt SE3 | Stdev |
| Li | 3.5 | 0.3 | 13 | 1 | 0.27 | 0.03 |
| Sc | 315 | 151 | 1815 | 45 | 0.17 | 0.08 |
| Mn | 102 | 34 | 482 | 4 | 0.21 | 0.07 |
| Co | 298 | 157 | 1852 | 96 | 0.16 | 0.09 |
| Ni | 158 | 90 | 977 | 47 | 0.16 | 0.09 |
| Ga | 196 | 104 | 1125 | 64 | 0.17 | 0.09 |

Table 4 (continued)

| n | SE_Pyro3 | | 5 | | D Nb-pyr/melt SE3 | Stdev |
|----|----------|--------|---------|-------|-------------------|-------|
| | Nb-pyr | Stdev | Melt | stdev | | |
| Ge | 40 | 3 | 50 | 28 | 0.8 | 0.5 |
| Sr | 547 | 10 | 618 | 12 | 0.88 | 0.02 |
| Y | 893 | 53 | 1400 | 60 | 0.64 | 0.05 |
| Zr | 697 | 139 | 2050 | 74 | 0.34 | 0.07 |
| Nb | 489,667 | 38,502 | 273,134 | 6537 | 1.8 | 0.1 |
| Mo | 10 | 1 | 27 | 5 | 0.37 | 0.09 |
| Ba | 265 | 68 | 944 | 18 | 0.28 | 0.07 |
| La | 1895 | 259 | 911 | 74 | 2 | 0.3 |
| Ce | 994 | 70 | 670 | 34 | 1.5 | 0.1 |
| Nd | 2376 | 314 | 1223 | 82 | 1.9 | 0.3 |
| Sm | 1791 | 169 | 1098 | 56 | 1.6 | 0.2 |
| Gd | 843 | 55 | 678 | 34 | 1.2 | 0.1 |
| Dy | 665 | 18 | 737 | 34 | 0.9 | 0.05 |
| Yb | 396 | 51 | 820 | 30 | 0.48 | 0.06 |
| Lu | 762 | 133 | 1847 | 81 | 0.41 | 0.07 |
| Hf | 901 | 105 | 1980 | 116 | 0.45 | 0.06 |
| Ta | 4361 | 947 | 1142 | 100 | 3.8 | 0.9 |
| Th | 167 | 6 | 196 | 11 | 0.85 | 0.06 |
| U | 23 | 12 | 108 | 31 | 0.2 | 0.1 |
| n | SE_Pyro4 | | 5 | | D Nb-pyr/melt SE4 | Stdev |
| | Nb-pyr | Stdev | melt | Stdev | | |
| Li | 5.3 | 0.4 | 11.7 | 0.5 | 0.97 | 0.09 |
| Sc | 551 | 182 | 1822 | 18 | 0.82 | 0.27 |
| Mn | 127 | 59 | 514 | 3 | 0.7 | 0.3 |
| Co | 363 | 270 | 2034 | 52 | 0.58 | 0.43 |
| Ni | 188 | 125 | 1032 | 25 | 0.6 | 0.4 |
| Ga | 196 | 147 | 1008 | 23 | 0.5 | 0.4 |
| Ge | 123 | 67 | 288 | 191 | 2.3 | 2.0 |
| Sr | 568 | 18 | 606 | 18 | 1.31 | 0.06 |
| Y | 825 | 168 | 1421 | 24 | 1.10 | 0.20 |
| Zr | 1180 | 190 | 2058 | 47 | 1.20 | 0.20 |
| Nb | 481,096 | 60,016 | 268,189 | 9708 | 1.50 | 0.20 |
| Mo | 8.5 | 0.8 | 18 | 4 | 0.8 | 0.2 |
| Ba | 339 | 108 | 962 | 20 | 0.9 | 0.3 |
| La | 1916 | 147 | 841 | 21 | 1.6 | 0.1 |
| Ce | 932 | 59 | 643 | 10 | 1.43 | 0.09 |
| Nd | 2359 | 141 | 1176 | 28 | 1.6 | 0.1 |
| Sm | 1681 | 94 | 1065 | 21 | 1.47 | 0.09 |
| Gd | 784 | 73 | 668 | 13 | 1.40 | 0.10 |
| Dy | 609 | 91 | 739 | 15 | 1.20 | 0.20 |
| Yb | 379 | 118 | 835 | 14 | 0.90 | 0.30 |
| Lu | 753 | 279 | 1919 | 64 | 0.90 | 0.30 |
| Hf | 1561 | 247 | 1997 | 70 | 1.4 | 0.2 |
| Ta | 3862 | 1055 | 1084 | 85 | 1.6 | 0.5 |

Table 4 (continued)

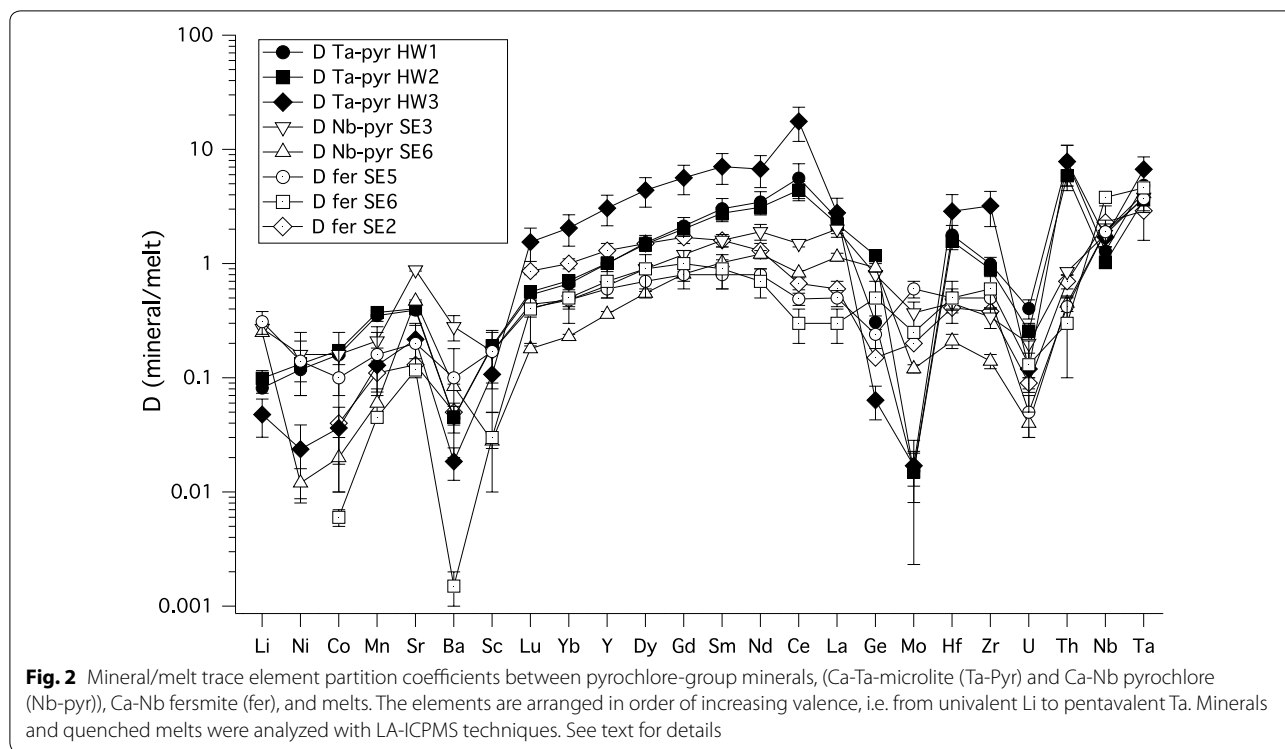
| SE_Pyro4 | | | | | | | | | | |
|-----------------|---------------|--------------|-------------|--------------|--------------------------|--------------|--------------------------|--------|-----------------------|--------|
| n | 5 | | 5 | | D Nb-pyr/melt SE4 | Stdev | | | | |
| | Nb-pyr | Stdev | melt | Stdev | | | | | | |
| Th | 199 | 22 | 189 | 4 | 1.41 | 0.2 | | | | |
| U | 38 | 25 | 133 | 44 | 0.91 | 0.7 | | | | |
| SE_Pyro5 | | | | | | | | | | |
| n | 5 | | 5 | | D fer/melt SE5 | Stdev | | | | |
| | Fer | Stdev | melt | Stdev | | | | | | |
| Li | 4.2 | 1.0 | 13.6 | 0.5 | 0.31 | 0.07 | | | | |
| Sc | 388 | 214 | 2292 | 14 | 0.17 | 0.09 | | | | |
| Mn | 94 | 57 | 602 | 5 | 0.16 | 0.09 | | | | |
| Co | 328 | 253 | 2281 | 24 | 0.1 | 0.08 | | | | |
| Ni | 160 | 84 | 1144 | 14 | 0.14 | 0.07 | | | | |
| Ga | 187 | 145 | 1194 | 12 | 0.2 | 0.1 | | | | |
| Ge | 13 | 2 | 51 | 9 | 0.24 | 0.06 | | | | |
| Sr | 175 | 76 | 736 | 16 | 0.20 | 0.10 | | | | |
| Y | 918 | 166 | 1609 | 40 | 0.60 | 0.10 | | | | |
| Zr | 1269 | 248 | 2462 | 81 | 0.50 | 0.10 | | | | |
| Nb | 474,314 | 123,606 | 253,661 | 11,699 | 1.9 | 0.5 | | | | |
| Mo | 13 | 3 | 20 | 0 | 0.6 | 0.1 | | | | |
| Ba | 178 | 138 | 1187 | 39 | 0.1 | 0.08 | | | | |
| La | 483 | 74 | 973 | 35 | 0.5 | 0.08 | | | | |
| Ce | 349 | 44 | 719 | 19 | 0.49 | 0.06 | | | | |
| Nd | 1034 | 185 | 1262 | 34 | 0.8 | 0.1 | | | | |
| Sm | 973 | 207 | 1145 | 27 | 0.8 | 0.2 | | | | |
| Gd | 611 | 137 | 725 | 19 | 0.8 | 0.2 | | | | |
| Dy | 582 | 133 | 818 | 28 | 0.7 | 0.2 | | | | |
| Yb | 454 | 75 | 950 | 31 | 0.48 | 0.08 | | | | |
| Lu | 967 | 137 | 2200 | 74 | 0.44 | 0.06 | | | | |
| Hf | 1334 | 288 | 2501 | 91 | 0.5 | 0.1 | | | | |
| Ta | 2973 | 749 | 812 | 33 | 3.7 | 0.9 | | | | |
| Th | 95 | 20 | 227 | 7 | 0.42 | 0.09 | | | | |
| U | 9 | 3 | 163 | 12 | 0.05 | 0.02 | | | | |
| SE_Pyro6 | | | | | | | | | | |
| n | 5 | | 2 | | 5 | | D Nb-pyr/melt SE6 | | D fer/melt SE6 | |
| | Nb-pyr | Stdev | Fer | Stdev | Melt | Stdev | | | | |
| Li | 3 | – | – | – | 10.3 | 0.2 | 0.25 | – | – | – |
| Sc | 62 | 9 | 70 | 51 | 2240 | 11 | 0.028 | 0.004 | 0.03 | 0.02 |
| Mn | 33 | 9 | 26 | 2 | 570 | 5 | 0.06 | 0.02 | 0.045 | 0.0003 |
| Co | 43 | 22 | 14 | 3 | 2191 | 24 | 0.02 | 0.01 | 0.006 | 0.001 |
| Ni | 13 | 5 | – | – | 1115 | 14 | 0.012 | 0.004 | – | – |
| Ga | 6.6 | 1.1 | 1.2 | 0.5 | 1286 | 19 | 0.0051 | 0.0009 | 0.001 | 0.0004 |
| Ge | 22 | 2 | 13 | 4 | 23.6 | 1.0 | 0.92 | 0.08 | 0.5 | 0.2 |
| Sr | 366 | 7 | 92 | 3 | 781 | 15 | 0.47 | 0.01 | 0.117 | 0.005 |
| Y | 555 | 20 | 1001 | 314 | 1539 | 30 | 0.36 | 0.02 | 0.7 | 0.2 |
| Zr | 319 | 39 | 1372 | 439 | 2300 | 45 | 0.14 | 0.02 | 0.6 | 0.2 |
| Nb | 398,834 | 6729 | 803,171 | 23,398 | 209,001 | 6675 | 1.91 | 0.07 | 3.8 | 0.2 |

Table 4 (continued)

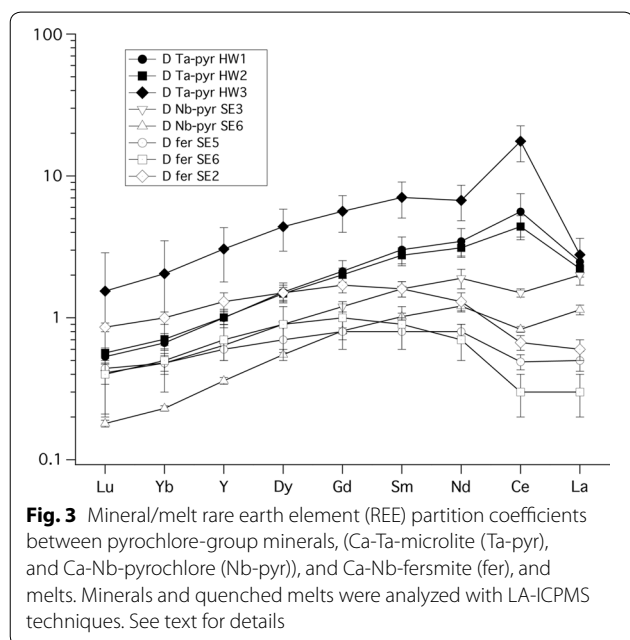
| n | SE_Pyro6 | | 2 | 5 | 5 | Stdev | D Nb-pyr/ melt SE6 | D fer/melt SE6 | | |
|----|----------|--------|------|-----|------|-------|-----------------------|----------------|--------|--------|
| | 5 | Nb-pyr | | | | | | | | |
| Mo | 5.7 | 0.5 | 11.9 | 0.6 | 47.8 | 1.0 | 0.12 | 0.01 | 0.25 | 0.01 |
| Ba | 98 | 4 | 1.7 | 0.5 | 1167 | 29 | 0.084 | 0.004 | 0.0015 | 0.0005 |
| La | 1439 | 109 | 343 | 143 | 1265 | 27 | 1.14 | 0.09 | 0.3 | 0.1 |
| Ce | 712 | 31 | 282 | 126 | 858 | 21 | 0.83 | 0.04 | 0.3 | 0.1 |
| Nd | 1824 | 125 | 1089 | 361 | 1504 | 32 | 1.21 | 0.09 | 0.7 | 0.2 |
| Sm | 1291 | 75 | 1119 | 353 | 1266 | 30 | 1.02 | 0.06 | 0.9 | 0.3 |
| Gd | 597 | 25 | 742 | 214 | 738 | 16 | 0.81 | 0.04 | 1.0 | 0.3 |
| Dy | 434 | 12 | 682 | 207 | 796 | 20 | 0.55 | 0.02 | 0.9 | 0.3 |
| Yb | 208 | 8 | 448 | 170 | 908 | 22 | 0.23 | 0.01 | 0.5 | 0.2 |
| Lu | 380 | 19 | 896 | 333 | 2128 | 47 | 0.18 | 0.01 | 0.4 | 0.2 |
| Hf | 484 | 63 | 1180 | 579 | 2343 | 53 | 0.21 | 0.03 | 0.5 | 0.2 |
| Ta | 4050 | 593 | 4490 | 497 | 985 | 18 | 4.1 | 0.6 | 4.6 | 0.5 |
| Th | 108 | 16 | 64 | 54 | 241 | 5 | 0.45 | 0.07 | 0.3 | 0.2 |
| U | 2.9 | 0.8 | 11 | 6 | 81 | 4 | 0.04 | 0.01 | 0.13 | 0.08 |

| n | SE_Pyro2 | | 5 | Stdev | D fer/melt SE2 | | |
|----|----------|--------|---------|-------|----------------|-------|--|
| | 2 | Fer | | | | | |
| Li | – | – | 11.2 | 0.2 | – | – | |
| Sc | – | – | 3.0 | 0.04 | – | – | |
| Mn | 2.5 | – | 22.7 | 0.5 | 0.11 | – | |
| Co | 1.3 | 0.4 | 32.6 | 0.4 | 0.04 | – | |
| Ni | – | – | 85.6 | 3.3 | – | – | |
| Ga | – | – | 4.4 | 0.2 | – | – | |
| Ge | 2.6 | – | 17.6 | 0.3 | 0.15 | – | |
| Sr | 15.6 | 1.9 | 123 | 1 | 0.13 | – | |
| Y | 5.5 | 0.44 | 4.1 | 0.1 | 1.3 | 0.2 | |
| Zr | 31 | 12 | 80 | 1 | 0.38 | 0.03 | |
| Nb | 583,356 | 17,353 | 253,850 | 3380 | 2.3 | 0.9 | |
| Mo | 10.4 | 0.9 | 52.3 | 0.9 | 0.2 | 0.007 | |
| Ba | 0.7 | 0.2 | 13.5 | 0.4 | 0.05 | 0.01 | |
| La | 1.6 | 0.2 | 2.55 | 0.04 | 0.6 | 0.1 | |
| Ce | 2.5 | 0.3 | 3.8 | 0.1 | 0.67 | 0.08 | |
| Nd | 3.4 | 0.4 | 2.5 | 0.1 | 1.3 | 0.2 | |
| Sm | 8.8 | 0.9 | 5.5 | 0.1 | 1.6 | 0.2 | |
| Gd | 3.1 | 0.4 | 1.8 | 0.1 | 1.7 | 0.2 | |
| Dy | 2.5 | 0.3 | 1.7 | 0.1 | 1.5 | 0.2 | |
| Yb | 1.8 | 0.1 | 1.9 | 0.1 | 1.0 | 0.1 | |
| Lu | 1.7 | 0.2 | 1.9 | 0.1 | 0.86 | 0.06 | |
| Hf | 1.2 | 0.6 | 3.0 | 0.1 | 0.41 | 0.04 | |
| Ta | 39.6 | 0.8 | 13.5 | 0.1 | 2.9 | 1.3 | |
| Th | 0.8 | 0.1 | 1.14 | 0.04 | 0.7 | 0.1 | |
| U | 0.28 | 0.04 | 3.08 | 0.03 | 0.09 | 0.01 | |

Fer = Ca-Nb-fernsite, Nb-pyr = Ca-Nb-pyrochlore, melt = quenched melt, Ta-pyr = Ca-Ta-microlite, stdev = standard deviation (2 sigma)



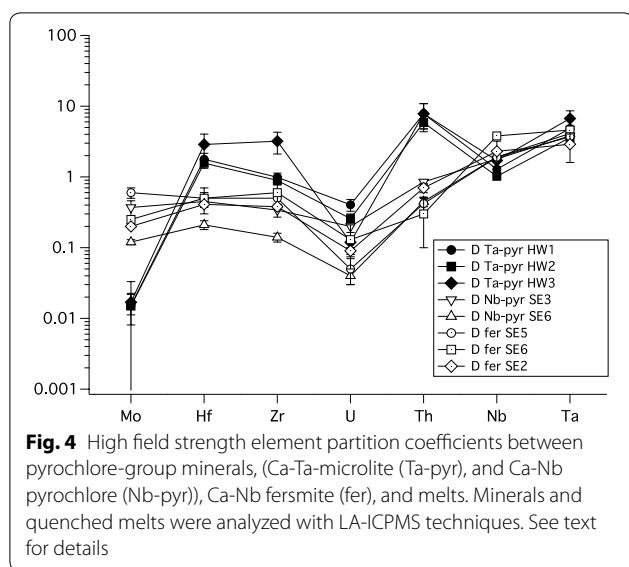
does occur as Ce^{4+} and Ce^{3+} . Whilst most trivalent REE occupy the A-site (i.e. the Ca-site) in pyrochlores, it could be that the smaller Ce^{4+} ion (ionic radius of 0.87 Å [46]) can also occupy the B-site, which is mainly occupied by pentavalent Nb and Ta. More crystallographic data on pyrochlores would be needed to confirm this notion.



However, the D's (pyrochlore/melt) in runs with the SE-pyro starting material, which contains F, show no positive Ce-anomaly (Fig. 3), and D (fersmite/melt) with SE-pyro also show only a very weak positive Ce anomaly. We speculate that this behavior may be caused by F in the melt, which may form stable complexes with Ce^{4+} , i.e. similar to CeF_8^{4-} or CeF_6^{2-} type compounds that have been reported in experiments with aqueous solutions [47]. These complexes in the melt would lead to an increased partitioning of Ce^{4+} into the melt, which consequently lowers D_{Ce} mineral/melt in F-bearing runs (Fig. 3).

As to the high field strength elements (HFSE), we find that the HFSE partition coefficients for Nb and Ta are above unity (Table 4), and other D_{HFSE} (Th, Zr, Hf, U, Mo) vary with bulk composition and temperature (Fig. 4). D_{Ta} is very similar to D_{Nb} , but overall we find that D_{Ta} are systematically higher than D_{Nb} , which is in good agreement with previous data for perovskite, rutile and other Ti-rich oxide minerals [2, 3, 5, 7, 8, 10, 13, 48–50]. Our data shows that D_{HFSE} for Ta-pyrochlore (HW1-3) are mostly above 1, only D_{Mo} in the HW runs are systematically below 1. The Zr and Hf partition coefficients are close to 1, with D_{Zr} and D_{Hf} slightly higher than 1 for Ta-rich microlite, and D_{Zr} and D_{Hf} are slightly lower than 1 for Nb-pyrochlore and fersmite (Table 4).

This compatible in Ta-rich microlite with a partition coefficient of almost 10, c.f., Table 4). Although one



might expect U to exhibit similar partitioning behavior as Th, we find that U is slightly incompatible in pyrochlore, microlite and fersmite (Table 4). This can be readily explained by the oxidizing conditions prevailing in our 1-atm experiments, under which U ions occur mainly in the 6+ valence state and, thus, do not fit as well into the mineral structures as U^{4+} would [8, 10]. As Th^{4+} (ionic radius of 0.94 Å) and U^{6+} (with its ionic radius of 0.89 Å in octahedral coordination [46]) are too large to replace Nb or Ta (ionic radius of 0.64 Å [46]) in pyrochlore-group minerals, we presume that both elements partition into the Ca-sites (ionic radius of Ca is 1.0 Å in octahedral coordination), despite the large charge difference.

Implications

To interpret the trace element budget of alkaline-rich und undersaturated melts, one needs to understand the trace element partitioning of all mineral phases involved. In the next paragraph we will show some important aspects of how crystallizing pyrochlore-group minerals may affect coexisting melt compositions. Note that our experiments were done in silicate melt systems, and as no other data are available, we assume that our results are also applicable to carbonate melt systems.

Our data show that pyrochlores prefer to incorporate Th over U ($D_{Th} > D_U$) under oxidizing conditions; hence crystallization of pyrochlore will deplete a melt in Th and enrich it in U. The composition of natural pyrochlores varies dramatically, but many primitive pyrochlores contain superchondritic Th/U (e.g., [51]), which may be caused by the aforementioned uneven partitioning of Th and U. If natural pyrochlores contain a lot more U than Th (e.g. [15]) then either the melt must have had

exceptionally high U/Th [52], or, perhaps more common, the pyrochlores were precipitated from or altered by a hydrothermal fluid, which can transport U much more efficiently than Th [15]. A recent paper shows nicely how the U and Th composition of pyrochlore varies with increasing degree of alteration: Whereas primitive pyrochlores contain wt.% of Th and only little U, the U content of pyrochlore increases and the Th content decreases with increasing degree of hydrothermal alteration [51].

Carbonatite and undersaturated silicate rocks are often extremely enriched in REE, so that many carbonatites are mined for the REE. As pyrochlores prefer to incorporate the lighter REE over the heavier ones ($D_{LREE} > D_{HREE}$), precipitation of pyrochlore minerals from a melt will lower the light REE concentrations (i.e., La, Ce, etc.) significantly, whereas the concentrations of the heavier REE (e.g., Yb, Lu) will not be depleted so much ($D_{HREE} \approx 1$). This may explain why primary bastnäsite, a Ce-carbonate, is scarce in carbonatites [26], and only secondary hydrothermal alteration (and breakdown of pyrochlores) may lead to the formation of the formation of REE-carbonates.

Conclusions

We present hitherto unknown experimentally determined trace element partition coefficients between pyrochlore, microlite, fersmite, and silicate melts. The partition coefficients show that pyrochlore, microlite, and fersmite can fractionate U from Th during differentiation of a magma under oxidizing conditions. Furthermore, our REE partition coefficients reveal that pyrochlores prefer to incorporate the lighter REE over the heavy REE, and this may prevent the crystallization of REE-carbonates in many carbonatite melts.

Acknowledgements

We would like to thank R. Nielsen and an anonymous reviewer for constructive reviews, which helped to significantly improve our manuscript. Our thanks go to the members of the workshops and the laboratories at the University of Münster, especially M. Trogisch, M. Feldhaus, P. Weitkamp, V. Rapelius, and B. Schmitte. Furthermore, we would like to extend our thanks to H. Wallat and S. Grund, who helped with some of the experiments and the analyses, and J. Schwenne who helped with the data reduction.

Authors' contributions

SK designed the study, wrote the manuscript, and processed the data. JB analyzed major and trace elements, wrote the manuscript, and processed the data. All authors read and approved the final manuscript.

Funding

We did not receive third party funding for the research presented here. Open access funding provided by Projekt DEAL.

Availability of data and materials

The dataset supporting the conclusions of this article is included within the article.

Competing interests

The authors declare that they have no competing interests.

Received: 15 June 2020 Accepted: 28 July 2020
Published online: 24 August 2020

References

- Green TH (1994) Experimental studies of trace-element partitioning applicable to igneous petrogenesis—Sedona 16 years later. *Chem Geol* 117(1–4):1–36
- Foley SF, Barth MG, Jenner GA (2000) Rutile/melt partition coefficients for trace elements and an assessment of the influence of rutile on the trace element characteristics of subduction zone magmas. *Geochim Cosmochim Acta* 64(5):933–938
- Holycross M, Cottrell E (2020) Partitioning of V and 19 other trace elements between rutile and silicate melt as a function of oxygen fugacity and melt composition: implications for subduction zones. *Am Mineral* 105(2):244–254
- Klemme S, Dalpe C (2003) Trace-element partitioning between apatite and carbonatite melt. *Am Mineral* 88(4):639–646
- Klemme S, Günther D, Hametner K, Prowatke S, Zack T (2006) The partitioning of trace elements between ilmenite, ulvöspinel, armalcolite and silicate melts with implications for the early differentiation of the moon. *Chem Geol* 234(3–4):251–263
- Klemme S, Meyer HP (2003) Trace element partitioning between baddeleyite and carbonatite melt at high pressures and high temperatures. *Chem Geol* 199(3–4):233–242
- Xiong XL, Adam J, Green TH (2005) Rutile stability and rutile/melt HFSE partitioning during partial melting of hydrous basalt: Implications for TTG genesis. *Chem Geol* 218(3–4):339–359
- Klemme S, Prowatke S, Hametner K, Günther D (2005) Partitioning of trace elements between rutile and silicate melts: implications for subduction zones. *Geochim Cosmochim Acta* 69(9):2361–2371
- Loroch D, Klemme S, Berndt J, Rohrbach A (2018) Experimentally determined trace element partition coefficients between hibonite, melilite, spinel, and silicate melts. *Data Brief* 21:2447–2463
- Prowatke S, Klemme S (2005) Effect of melt composition on the partitioning of trace elements between titanite and silicate melt. *Geochim Cosmochim Acta* 69(3):695–709
- Wijbrans CH, Klemme S, Berndt J, Vollmer C (2015) Experimental determination of trace element partition coefficients between spinel and silicate melt: the influence of chemical composition and oxygen fugacity. *Contrib Mineral Petrol* 169:4
- Prowatke S, Klemme S (2006) Rare earth element partitioning between titanite and silicate melts: Henry's law revisited. *Geochim Cosmochim Acta* 70(19):4997–5012
- Beyer C, Berndt J, Tappe S, Klemme S (2013) Trace element partitioning between perovskite and kimberlite to carbonatite melt: New experimental constraints. *Chem Geol* 353:132–139
- Auricchio C, De Vito C, Ferrini V, Orlandi P (2002) Nb and Ta oxide minerals in the Fonte del Prete granitic pegmatite dike, Island of Elba, Italy. *Can Min* 40:799–814
- Finch AA, McCreath JA, Reekie CDJ, Hutchison W, Ismaila A, Armour-Brown A, Andersen T, Simonsen SL (2019) From mantle to Motzfeldt: a genetic model for syenite-hosted Ta Nb-mineralisation. *Ore Geol Rev* 107:402–416
- McCreath JA, Finch AA, Herd DA, Armour-Brown A (2013) Geochemistry of pyrochlore minerals from the Motzfeldt Center, South Greenland: the mineralogy of a syenite-hosted Ta Nb deposit. *Am Mineral* 98(2–3):426–438
- Kryvdik SG, Sharygin VV, Dubyna OV, Morgun VG, Tomurko LL (2018) Ta-Nb Mineralization in the alkaline rocks of the eastern azov area (Ukraine). *Mineral J Ukraine* 40(3):39–64
- Mitchell RH (2015) Primary and secondary niobium mineral deposits associated with carbonatites. *Ore Geol Rev* 64:626–641
- Ohnenstetter D, Piantone P (1992) Pyrochlore-group minerals in the beauvoir peraluminous leukogranite, massif-central. *France Can Min* 30:771–784
- Savelyeva VB, Bazarova EP, Khromova EA, Kanakin SV (2018) REE minerals in the rocks of the Katugin rare metal deposit, east Transbaikalia: behavior of lanthanides and Y during crystallization of an F-saturated apatitic melt. *Geol Ore Dep* 60(8):643–657
- Chakhmouradian AR (1996) On the development of niobium and rare-earth minerals in monticellite-calcite carbonatite of the Oka complex. *Quebec Can Min* 34:479–484
- Chakhmouradian AR (2006) High-field-strength elements in carbonatitic rocks: geochemistry, crystal chemistry and significance for constraining the sources of carbonatites. *Chem Geol* 235(1–2):138–160
- Chakhmouradian AR, Reguir EP, Kressall RD, Crozier J, Pisiak LK, Sidhu R, Yang P (2015) Carbonatite-hosted niobium deposit at Aley, northern British Columbia (Canada): mineralogy, geochemistry and petrogenesis. *Ore Geol Rev* 64:642–666
- Steenfelt A (1991) High-technology metals in alkaline and carbonatitic rocks in Greenland—recognition and exploration. *J Geochem Explor* 40(1–3):263–279
- Krishnamurthy P, Hoda SQ, Sinha RP, Banerjee DC, Dwivedy KK (2000) Economic aspects of carbonatites of India. *J Asian Earth Sci* 18(2):229–235
- Cordeiro PFD, Brod JA, Palmieri M, de Oliveira CG, Barbosa ESR, Santos RV, Gaspar JC, Assis LC (2011) The Catalao I niobium deposit, central Brazil: resources, geology and pyrochlore chemistry. *Ore Geol Rev* 41(1):112–121
- Mackay DAR, Simandl GJ (2015) Pyrochlore and columbite-tantalite as indicator minerals for specialty metal deposits. *Geochem Expl Environ* 15(2–3):167–178
- Hogarth DD (1977) Classification and nomenclature of the pyrochlore group. *Am Mineral* 62:403–410
- Atencio D, Andrade MB, Christy AG, Giere R, Kartashov PM (2010) The pyrochlore supergroup of minerals: nomenclature. *Can Min* 48(3):673–698
- Barbosa ESR, Brod JA, Cordeiro PFO, Junqueira-Brod TC, Santos RV, Dantas EL (2020) Phoscorites of the salitre I complex: origin and petrogenetic implications. *Chem Geol* 535:119463
- Torro L, Villanova C, Castillo M, Campeny M, Goncalves AO, Melgarejo JC (2012) Niobium and rare earth minerals from the Virulundo carbonatite, Namibe, Angola. *Min Mag* 76(2):393–409
- Williams CT (1996) The occurrence of niobian zirconolite, pyrochlore and baddeleyite in the Kovdor carbonatite complex, Kola Peninsula, Russia. *Min Mag* 60(401):639–646
- Williams CT, Wall F, Woolley AR, Phillip S (1997) Compositional variation in pyrochlore from the Bingo carbonatite, Zaire. *J Afr Earth Sci* 25(1):137–145
- Cerny P, Chapman R, Ferreira K, Smeds SA (2004) Geochemistry of oxide minerals of Nb, Ta, Sn, and Sb in the Varutrask granitic pegmatite, Sweden: The case of an "anomalous" columbite-tantalite trend. *Am Mineral* 89(4):505–518
- Donaldson CH, Williams RJ, Lofgren G (1975) A sample holding technique for study of crystal growth in silicate melts. *Am Mineral* 60:324–326
- Borisov A (2001) Loop technique: dynamics of metal/melt equilibration. *Mineral Petrol* 71(1–2):87–94
- Sossi PA, Klemme S, O'Neill HS, Berndt J, Moynier F (2019) Evaporation of moderately volatile elements from silicate melts: experiments and theory. *Geochim Cosmochim Acta* 260:204–231
- Klemme S, Prowatke S, Münker C, Magee C, Lahaye Y, Zack T, Kasemann S, Cabato E, Kaeser B (2008) Synthesis and preliminary characterisation of new silicate, phosphate and titanite reference glasses. *Geost Geoanal Res* 32(1):39–54
- Jochum KP, Nohl U, Herwig K, Lammel E, Stoll B, Hofmann AW (2005) GeoReM: a new geochemical database for reference materials and isotopic standards. *Geost Geoanal Res* 29(3):333–338
- Griffin WL, Powell WJ, Pearson NJ, O'Reilly SY (2008) GLITTER: data reduction software for laser ablation ICP-MS in the earth sciences. In: Sylvester P (ed) *Laser Ablation-ICP-MS in the Earth Sciences; Current practices and outstanding issues*. Short course series, Vol 40. Mineralogical Association of Canada, Vancouver, BC, pp 308–311
- Prowatke S, Klemme S (2006) Rare earth element partitioning between titanite and silicate melts: Henry's law revisited. *Geochim Cosmochim Acta* 70:4997–5012
- Perrault G (1968) La composition chimique et la structure cristalline du pyrochlore d'Oka, P.Q. *Can Min* 9:383–402
- Gasparin M (1955) Synthèse et identification de deux oxydes doubles de tantalite et d'étain. *Compt Rendus Sci* 240:2340–2342
- Prowatke S, Klemme S (2006) Trace element partitioning between apatite and silicate melts. *Geochim Cosmochim Acta* 70(17):4513–4527

45. Cummings JP, Simonsen SH (1970) The crystal structure of calcium niobate (CaNb₂O₆). *Am Mineral* 55:90–97
46. Shannon RD (1976) Revised effective ionic radii and systematic studies of interatomic distances in halides and chalcogenides. *Acta Crystallographica A* 32:751–767
47. Marsac R, Réal F, Banik N, Pédrot M, Pourret O, Vallet V (2017) Aqueous chemistry of Ce(IV): estimations using actinide analogues. *Dalton Trans* 46:13553–13561
48. Green TH, Pearson NJ (1987) An experimental study of Nb and Ta partitioning between Ti-rich minerals and silicate liquids at high pressure and temperature. *Geochim Cosmochim Acta* 51:55–62
49. Horn J, Foley SF, Jackson SE, Jenner GA (1994) Experimentally determined partitioning of high field strength- and selected transition elements between spinel and basaltic melt. *Chem Geol* 117:193–218
50. Nielsen RL, Beard JS (2000) Magnetite-melt HFSE partitioning. *Chem Geol* 164:21–34
51. Khromova EA, Doroshkevich AG, Sharygin VV, Izbrodin LA (2017) Compositional evolution of pyrochlore-group minerals in carbonatites of the belaya zima pluton, Eastern Sayan. *Geol Ore Dep* 59(8):752–764
52. Lee MJ, Lee JI, Garcia D, Moutte J, Williams CT, Wall F, Kim Y (2006) Pyrochlore chemistry from the Sokli phosphorite-carbonatite complex, Finland: implications for the genesis of phosphorite and carbonatite association. *Geochem J* 40(1):1–13

Publisher's Note

Springer Nature remains neutral with regard to jurisdictional claims in published maps and institutional affiliations.

Ready to submit your research? Choose BMC and benefit from:

- fast, convenient online submission
- thorough peer review by experienced researchers in your field
- rapid publication on acceptance
- support for research data, including large and complex data types
- gold Open Access which fosters wider collaboration and increased citations
- maximum visibility for your research: over 100M website views per year

At BMC, research is always in progress.

Learn more biomedcentral.com/submissions

